

NASA  
TP  
1795  
c.1

# NASA Technical Paper 1795

LOAN COPY:  
AFWL TECHN  
KIRTLAND AI

TECH LIBRARY KAFB, NM  
0067635

## Effects of Temperature, Thermal Exposure, and Fatigue on an Alumina/Aluminum Composite

George C. Olsen

DECEMBER 1980





NASA Technical Paper 1795

# Effects of Temperature, Thermal Exposure, and Fatigue on an Alumina/Aluminum Composite

George C. Olsen  
*Langley Research Center*  
*Hampton, Virginia*

**NASA**

National Aeronautics  
and Space Administration

**Scientific and Technical  
Information Branch**

1980

## SUMMARY

The effects of thermal exposure and mechanical fatigue on the properties of a composite material composed of aluminum matrix unidirectionally reinforced with polycrystalline alumina ( $\alpha\text{Al}_2\text{O}_3$ ) fibers were experimentally evaluated. Some specimens were isothermally exposed for up to 10 000 hours at 590 K, while others were thermally cycled between 200 K and 590 K for 6000 cycles. As-fabricated specimens and thermally exposed specimens were exposed to  $10^6$  tension-tension fatigue cycles. Strengths and elastic moduli of the as-fabricated material and the effects of thermal and fatigue exposure on them were determined by mechanically testing the specimens. The effects of fabrication, thermal exposure, and mechanical fatigue on the microstructure of the material were evaluated with metallurgical techniques such as scanning electron microscopy, optical microscopy, and X-ray diffraction.

Tests showed that fiber strength was severely degraded by the fabrication process, probably because of formation of vacancies and accompanying stress fields in the fiber near the surface during a surface reduction of alumina to a nonstoichiometric form. However, isothermal exposure at 590 K, thermal cycling, and fatigue cycling all restored the fibers' original strength by allowing the vacancies to be annihilated. Comparison of specific properties of the as-fabricated material with several other aerospace materials over the temperature range from 295 K to 590 K shows that it is an attractive candidate for select applications. Long duration isothermal exposure did not cause matrix-fiber reactions but did weaken the matrix by overaging and the diffusional loss of lithium to a surface reaction forming lithium carbonate. Thermal cycling caused some damage to the material by initiating cracks in the matrix which in turn induced some fiber failures. Tension-tension fatigue cycling between one-tenth and two-thirds of the ultimate tensile strength caused no apparent damage to the as-fabricated material but, in fact, strengthened it to the rule-of-mixtures value. Fatigue cycling after thermal exposure did have a cumulative damaging effect on the material.

## INTRODUCTION

Alumina is a well-characterized ceramic material (ref. 1) suitable for a broad range of applications. Reinforcement for metal matrix composites is one such application. Single-crystal whiskers, rods, and filaments of alumina have been used to reinforce aluminum, silver, copper, and nickel matrices (refs. 2, 3, and 4). However, limited availability and high cost of these forms of alumina have inhibited its widespread use in composite materials.

A high-volume low-cost process has been developed for making polycrystalline alumina ( $\alpha\text{Al}_2\text{O}_3$ ) fibers which are commercially available (ref. 5). Although this fiber does not have the high tensile strength of its single-crystal predecessors, it is chemically and thermally stable and has a high modulus of elasticity and moderate strength. These are attractive attributes

for composite material fabrication and applications. The matrix materials being considered for use with these polycrystalline alumina fibers include aluminum, magnesium, lead, resins, glass, and ceramics. This study addresses the alumina/aluminum composite system.

The alumina/aluminum composite system was consolidated with a liquid-metal infiltration technique. Aluminum by itself does not wet alumina; therefore, a small amount of lithium was added to the aluminum melt as a wetting agent. Because lithium has a lower surface free energy than aluminum, it concentrates at free surfaces of the melt and at interfaces between the matrix melt and fibers during fabrication. The actual wetting mode has not been determined, but considering the reactivity of lithium and its aggressive attack on alumina (ref. 1), wetting by formation of an intermetallic compound is the likely mechanism. Previous investigations of chemically extracted fibers have identified small amounts of lithium aluminum oxide ( $\text{LiAlO}_2$ ) on the fibers by X-ray diffraction (ref. 5) and of lithium spinel ( $\text{LiAl}_5\text{O}_8$ ) by electron diffraction (ref. 6). Lithium spinel has also been identified by X-ray diffraction of over-reacted fibers (ref. 7). Lithium may also form second phase  $\text{Al}_3\text{Li}$  particles in the aluminum matrix as reported in quenched lithium-aluminum alloys (refs. 8, 9, and 10).

This study of alumina/aluminum composite material had several purposes. One was to determine selected mechanical properties of the as-fabricated composite between room temperature and 590 K and compare them with properties of other well-characterized aerospace materials. Another purpose was to determine the effect of continuous long-term isothermal exposure and thermal cycling on the composite material. The final purpose was to determine the effect of mechanical fatigue on the composite material.

## MATERIALS AND EXPOSURE CONDITIONS

### Materials and Test Specimens

The composite material is an aluminum alloy matrix unidirectionally reinforced with 52 volume percent of alumina fiber. The continuous fibers are 99+ percent pure polycrystalline  $\alpha\text{Al}_2\text{O}_3$  with a diameter of 19.5  $\mu\text{m}$  (mean of 25 measurements). In their virgin state, they are white and have an ultimate strength of 1346 MPa (mean of 10 tests) and a reported elastic modulus of 379 GPa (ref. 5). The matrix material is 1100 aluminum alloy with 2.8 weight percent of lithium added to the melt to promote fiber wetting. In the annealed condition, lithium adds little to the 90 MPa strength of the aluminum but increases its modulus from 69 GPa to 76.5 GPa (ref. 11). Unidirectionally reinforced plates of the composite material were consolidated by the material supplier using a liquid-metal infiltration process. A mold was filled with aligned fibers held in place by a fugitive binder. A vacuum was drawn on the mold and held throughout the infiltration process. The mold was heated to burn off the fugitive binder and then submerged in a melt of the matrix material. After the mold reached thermal equilibrium with the melt, a seal was punctured

to allow the melt to infiltrate the mold and fibers. When fully infiltrated after approximately 5 minutes, the mold was removed from the melt and quenched with a water spray. The mold was then cut away leaving a composite plate approximately 150 mm × 200 mm × 25 mm. More detailed descriptions of the fiber and fabrication process are available in reference 5.

Test specimens, in the configurations listed in table I, were cut from the composite plates with a diamond cut-off wheel and finished with diamond surface grinding. Scanning electron microscopy of the machined edges revealed no fiber damage as a result of the machining. Prior to mechanical testing at room temperature, aluminum gripping tabs and strain gages were bonded with epoxy to the tension and compression specimens. Two gages were mounted back to back on the centerline to measure longitudinal strain, and a third gage was mounted to measure transverse strain. Tabs and strain gages on specimens to be tested at elevated temperature were bonded with high temperature ceramic base adhesives which required curing at 530 K for 5 hours. Sets of three replicate specimens were prepared for each test and exposure condition.

### Thermal Exposures

Continuous isothermal exposures.- Continuous isothermal exposures were conducted in an air-circulating electric oven. Sets of specimens were exposed at 590 K for 2500, 5000, and 10 000 hours. After removal from the oven, the specimens were allowed to cool in ambient air.

Cyclic thermal exposures.- Cyclic exposures were conducted in a dual chamber apparatus. Specimens, mounted on a mechanically driven sliding tray, were alternately inserted in an air-circulating, electrically heated hot chamber (590 K) and a liquid-nitrogen-cooled cold chamber (200 K). A full cycle was 10 minutes long with exposure of 7.3 minutes in the hot chamber and 2.7 minutes in the cold chamber required to obtain thermal equilibrium. A schematic drawing of the apparatus and a typical specimen temperature profile for one cycle are shown in figure 1. The specimens were exposed to this environment for 6000 cycles.

### Fatigue Conditioning

Three sets of longitudinal tensile specimens were mechanically fatigue conditioned: one set as-fabricated, one after 2500 hours at 590 K, and a third after 6000 thermal cycles. Fatigue conditioning was conducted at room temperature in a hydraulic testing machine. The testing machine, operated in a load control mode, loaded the specimens in a tension-tension sinusoidal cycle. Maximum load for the cycle was 11 kN (approximately two-thirds of the ultimate load for as-fabricated specimens) and the minimum load was 1.1 kN (one-tenth of the cycle maximum load). Specimens were conditioned for  $10^6$  cycles at 100 Hz with no significant specimen heating noted.

## TEST PROCEDURES

### Mechanical Property Tests

Composite specimens were tested in tension and compression. Test standards, method for determining shear modulus (ref. 12), properties reported, and cross-head speeds for these tests are shown in table II. (Symbols appearing in the tables and figures are defined in the appendix.) All tests were performed in air at atmospheric pressure in a 44.5 kN, mechanically driven test machine equipped with an environmental chamber for elevated-temperature tensile tests. Wedge grips were used for tensile tests, and an IITRI wedge grip fixture (described in ref. 13) was used for compression tests. Elevated-temperature compression specimens were heated with a clam shell electric resistance heater around the specimen gage length. Load cell and strain gage outputs for tension and compression tests were recorded and reduced on a digital computer system.

Individual fiber breaking loads were determined experimentally for virgin fibers and for fibers chemically removed from their composite matrix with a heated NaOH solution. Ten fibers from each group were tested on a bench-mounted fiber tensile tester. The motor-driven tester was equipped with a load cell and linearly variable displacement transducer. The load cell and displacement transducer outputs were recorded on an X-Y plotter. Fibers were centered in the 25 mm test section and attached with a thermoplastic adhesive.

### Metallurgical Analysis

Metallurgical analysis of the composite specimens included examination of fracture surfaces with scanning electron microscopy (SEM) and examination of polished and etched (with Keller's reagent) cross sections with optical microscopy. X-ray diffraction analysis was used to determine crystalline structure. Diffraction patterns were made using a copper  $K\alpha$  incident X-ray beam, a diffracted beam monochromator, a diffractometer, and a goniometer. Polished specimens were attached to an oscillating holder to reduce effects of preferred crystalline orientation. Additional analysis of fibers chemically removed from the composite matrix included thermogravimetric analysis, scanning differential calorimeter analysis with gaseous reaction product analysis, and X-ray diffraction of powdered samples.

## RESULTS AND DISCUSSION

Ultimate stresses and elastic moduli determined from each  $\alpha\text{Al}_2\text{O}_3/\text{Al}$  composite specimen tested are shown in tables III and IV. For each set of room-temperature data in these tables, the standard deviation as a percentage of the mean value did not exceed 7 percent. The standard deviation for the elevated-temperature tensile data was as high as 18 percent, and for the compression data, as high as 36 percent. High variability in elevated-temperature compression data is the result of limited test data and alignment perturbation by thermal expansion. All compression testing is alignment sensitive, but when elevated temperatures soften the matrix and reduce its side support of the fibers, the sensitivity is magnified. Reduction of the variability would

require more data and better elevated-temperature alignment control and would probably increase the mean values of compression strength.

#### As-Fabricated Material

Room-temperature properties.- Mean values of the as-fabricated material properties at room temperature (295 K) are shown in table V. The longitudinal tensile strength is 26 percent lower than would be expected from a rule-of-mixtures (ROM) calculation using the virgin fiber and matrix properties. Comparison of the strengths and moduli of the  $\alpha\text{Al}_2\text{O}_3/\text{Al}$  composite with those of a well-characterized B/Al composite (50 volume percent of 0.14-mm-diameter boron fibers in a 6061 aluminum matrix, ref. 14), shows its longitudinal tensile strength to be 37 percent lower than the B/Al. The longitudinal elastic modulus and the shear modulus of the two materials are the same. Properties of the  $\alpha\text{Al}_2\text{O}_3/\text{Al}$  composite that exceed those of B/Al include transverse tensile strength, 40 percent higher; transverse elastic modulus, 16 percent higher; and compressive strength, 76 percent higher. Compression loading of the  $\alpha\text{Al}_2\text{O}_3/\text{Al}$  composite specimens takes advantage of the inherently high compressive strength of the ceramic fibers; the composite's longitudinal compressive strength is approximately five times higher than its longitudinal tensile strength.

Fractographs from typical as-fabricated longitudinal and transverse tensile specimens are shown in figure 2. Longitudinal specimens failed in a noncumulative mode (ref. 15) characterized by flat surfaces with no fiber pullout or shear steps. The noncumulative failure model indicates a well-bonded composite with high interfacial shear strength. Transverse specimens failed by dimpled rupture of the matrix material with no indication of interface failure or fiber splitting.

X-ray diffraction patterns from the as-fabricated composite material were complex but provided correlation with every indexed peak for  $\alpha\text{Al}_2\text{O}_3$  (ASTM card no. 10-173) and aluminum (ASTM card no. 4-0787). One peak was unidentified. This peak could have originated from the 110 plane of a superlattice phase,  $\text{Al}_3\text{Li}$ , in the matrix. This phase is not easily identified by standard X-ray diffraction techniques but has been observed (refs. 8, 9, and 10) in quenched aluminum/lithium alloys. Reportedly, Guinier-Preston zones of  $\text{Al}_3\text{Li}$  nucleate and grow into small spherical particles in a matter of days at room temperature. No evidence of  $\text{LiAlO}_2$  or  $\text{LiAl}_5\text{O}_8$  was found in the composite material X-ray data. If the formation of either or both of these compounds is the wetting mechanism, the fabrication technique was successful in limiting their growth to regions so thin as to be undetectable by standard X-ray diffraction techniques.

An optical photomicrograph of a typical polished cross section from an as-fabricated specimen is shown in figure 3. No indication of matrix-fiber interaction is apparent in these cross sections. The variations in fiber diameter and spacing are typical for this material.

Fiber properties.- Fibers chemically removed from the composite matrix were dark gray. X-ray diffraction patterns from powdered samples of virgin fibers and chemically removed fibers correlated with every indexed peak for  $\alpha\text{Al}_2\text{O}_3$

(ASTM card no. 10-173) with an intensity greater than 5 percent. No other peaks were present in the patterns. The only difference was a half-maximum peak broadening of approximately 15 percent in the patterns from the chemically removed fibers compared with the patterns from the virgin fibers.

Thermogravimetric analysis (TGA) of the gray fiber in air at atmospheric pressure between room temperature and 900 K did not show any measurable weight change. However, the fiber sample changed back to its original white color during the test. Differential scanning calorimeter analysis (DSCA), including gaseous product analysis for temperatures up to 900 K, did not show any change in heat capacity or any gaseous products from the gray fiber. Again, the fiber returned to its original white color during the test. These data are inconclusive because they fail to indicate that the observed changes in fiber color are due to the formation and/or evaporation of a separate reaction product. However, color changes from white to gray have been observed previously (refs. 16, 17, 18, and 19) and were attributed to the formation of a nonstoichiometric alumina with a composition of approximately  $\text{Al}_2\text{O}_{2.96}$ . Reheating the gray nonstoichiometric alumina to 773 K in the presence of oxygen reportedly reoxidizes the alumina and restores its original white color as observed in the fiber TGA and DSCA tests. The formation of a nonstoichiometric alumina in the fibers is accompanied by an increase in vacancy density, which broadens the X-ray diffraction peaks as observed.

Individual fiber tensile tests for virgin fibers and fibers chemically removed from as-fabricated specimens show a 45-percent loss of fiber strength during the fabrication process. The reduced fiber strength correlates with the lower than expected longitudinal tensile strength of the as-fabricated composite material. Fibers lose strength during fabrication probably because of a high density of quenched-in vacancies in the fiber near the fiber surface caused by the reduction of alumina to a nonstoichiometric form. These vacancies increase the stress fields in the fibers and reduce fiber strength.

Effect of elevated test temperature.- As-fabricated  $\alpha\text{Al}_2\text{O}_3/\text{Al}$  composite specimens were mechanically tested at room temperature (295 K), 500 K, and 590 K. Results of the tests, the mean values normalized by dividing by the room-temperature mean values, are shown in figure 4. The fiber-dominated properties - ultimate longitudinal tensile strength and longitudinal elastic modulus - are nearly constant over the temperature range. Matrix-dominated properties - ultimate transverse tensile strength, transverse elastic modulus, ultimate longitudinal compression strength, and shear modulus - degraded with increasing temperature. The shaded area above the mean compression strength curve is bounded above by the maximum compression data obtained. If the elevated-temperature compression data variability previously discussed were eliminated, the material mean compression strength would probably lie in the neighborhood of the upper limit.

Several key properties of the  $\alpha\text{Al}_2\text{O}_3/\text{Al}$  composite were selected for comparison with other materials on a specific basis, i.e., the material property divided by the material density, for applications that are weight critical. The comparison materials include two aerospace alloys (ref. 20), Al 7075-T6 and Ti-6Al-4V (annealed), and three composite materials (ref. 14), 50 volume percent of boron fibers in a 6061 aluminum matrix (B/Al), 61 volume percent



of graphite fibers in an epoxy resin matrix (Gr/Ep), and 63 volume percent of graphite fibers in a polyimide resin matrix (Gr/PI). Because the fiber volume contents of these composites would not give a direct comparison, their properties and densities were scaled to an equivalent 52-volume-percent fiber content. The resulting scale factors for the specific properties were 1.04 for B/Al, 0.88 for Gr/Ep, and 0.84 for Gr/PI. Longitudinal properties were multiplied by the scale factors and transverse properties were divided by them. In addition, the maximum rated temperatures for the Gr/Ep and Gr/PI composites are 450 K and 533 K, respectively. The specific properties of these materials as a function of test temperature are shown in figure 5. Specific stiffness (fig. 5(a)) of the  $\alpha\text{Al}_2\text{O}_3/\text{Al}$  composite is several times higher than the alloys but slightly lower than the other composites. Specific transverse tensile strength (fig. 5(b)) of  $\alpha\text{Al}_2\text{O}_3/\text{Al}$  is similar to B/Al, about twice the value of the resin matrix composites, but much less than the alloys. Specific longitudinal tensile strength (fig. 5(c)) of  $\alpha\text{Al}_2\text{O}_3/\text{Al}$  is similar to the titanium but much less than the other composite materials. Specific longitudinal compression strength (fig. 5(d)) of  $\alpha\text{Al}_2\text{O}_3/\text{Al}$  is in the same range as the other composites and much higher than the alloys. As in the previous figure, the shaded area represents the probable increase in compression strength if testing variability is eliminated. These comparisons suggest that  $\alpha\text{Al}_2\text{O}_3/\text{Al}$  composite could be an attractive candidate for selected applications, ones for which specific stiffness, transverse tensile strength, and/or compression strength are critical, especially if material cost is a significant factor. Furthermore, if weight is not a limiting factor, the  $\alpha\text{Al}_2\text{O}_3/\text{Al}$  is more attractive because on an absolute basis, its stiffness, transverse tensile strength, and compression strength exceed the other composite materials considered.

### Thermal Exposure Effects

Continuous isothermal exposure.— Typical stress-strain curves for longitudinal and transverse tensile tests on  $\alpha\text{Al}_2\text{O}_3/\text{Al}$  composite specimens continuously exposed at 590 K for 2500, 5000, and 10 000 hours and tested at room temperature are shown in figure 6. Exposure for 2500 hours increased the longitudinal tensile strength by 14 percent but additional exposure for 5000 hours reduced it by 18 percent (to 6 percent below the as-fabricated strength). Further exposure, up to 10 000 hours, did not cause additional degradation of the longitudinal tensile strength. Transverse tensile strength was degraded 39, 58, and 62 percent by the 2500-, 5000-, and 10 000-hour exposures, respectively. Transverse strain-to-failure decreased in a similar manner. After 2500-hour exposure, compression strength decreased 17 percent and shear modulus increased 6 percent.

Isothermal exposure at 590 K in an air-circulating oven produced a tenacious dark gray reaction layer on the surface of the specimens. After 2500 hours, the reaction layer was thin; but after 5000 and 10 000 hours, the reaction layers were thick enough to scrape off powder samples. X-ray diffraction patterns made from these powder samples correspond to lithium carbonate ( $\text{Li}_2\text{CO}_3$ , ASTM card no. 22-1141). Formation of lithium carbonate on the surface requires diffusion of lithium from the bulk material for reaction with carbon dioxide and oxygen in the air. During fabrication some of the lithium in the matrix melt concentrates at the fiber-matrix interfaces, because it has lower

surface free energy and wets the fibers. Therefore, it is reasonable to assume that much, if not all, of the lithium diffusing to the surface comes from the area near the interface. The counterflux of vacancies from the surface therefore produces a concentration of microvoids near the interfaces.

Fracture surfaces of longitudinal tensile specimens became macroscopically rougher with increased thermal exposure. Microscopically, the fractographs (fig. 7) show some increase in surface roughness with respect to the planes of fiber fracture surfaces compared with the as-fabricated fracture surfaces (fig. 2). In addition, elevated tear ridges in the matrix and increased necking of matrix away from the fibers indicate that matrix ductility increased with increasing exposure time. Rougher fracture surfaces are an indication of degradation of the mechanism of load transfer between the matrix and the fibers. Transverse tensile fractographs (fig. 8) show similar effects. With increased thermal exposure, the transverse failures progressively occur at the fiber-matrix interface, in contrast with as-fabricated specimen failure in the matrix (fig. 2). The formation of dimples near the fiber surfaces (note especially the 10 000-hour specimen) indicate the coalescence of microvoids formed near the interface. Again, the elevated tear ridges and large dimples indicate increased matrix ductility, similar to that seen when precipitation-hardened aluminum alloys are overaged.

Fibers chemically removed from the composite matrix were individually tensile tested. Mean values and standard deviations of the breaking loads from 10 tests at each condition are shown in figure 9. These data show that fiber strength lost during fabrication is nearly restored to the virgin strength by isothermal exposure. Apparently thermal exposure enhances the movement and annihilation of the vacancies formed during fabrication.

These data indicate that mechanical property degradation due to long duration isothermal exposure at 590 K is a result of an interfacial diffusion phenomenon and not interfacial chemical reaction. Even when the material was exposed at extreme time-temperature conditions for aluminum alloys, 500 hours at 730 K, no interface reaction was observed (ref. 21) although strengths were severely degraded.

Cyclic thermal exposure.- Effects of 6000 thermal cycles between 200 K and 590 K on typical longitudinal and transverse tensile stress-strain curves of the composite material are shown in figure 10. Thermal cycling increased the longitudinal strength and elastic modulus of the material by 10 and 5 percent, respectively, and reduced the transverse tensile strength by 64 percent. After thermal cycling, there was no elastic region in the transverse stress-strain curves so no transverse modulus could be determined. Thermal cycling decreased compression strength and shear modulus, both matrix-dominated properties, by 31 and 48 percent, respectively (table IV).

Longitudinal and transverse tensile fractographs of the thermally cycled specimens are shown in figure 11. The longitudinal surface (fig. 11(a)) was rough with matrix shear steps, but very little bare fiber was exposed. Matrix material was still adhering to the fiber indicating that the interface was stronger than the matrix. The transverse fracture surface (fig. 11(b)) shows tear ridges between fibers and a dense population of small fragments of the

matrix attached to the fibers. These fragments appear to be the result of accumulated crack damage in the matrix incurred during thermal cycling. The angularity of the fragments suggests brittle failure probably occurring at the low temperature as a result of stresses induced by the differential in thermal expansion between the matrix and fiber.

Fibers chemically removed from a thermally cycled specimen and individually tensile tested showed the same strength restoration seen in the isothermally exposed specimens. These data indicate that thermal cycling causes matrix cracking which severely degrades transverse properties. During longitudinal mechanical loading, the matrix cracks induce stress concentrations in the fibers causing them to fail prematurely and partially offset the fiber strength restoration.

### Fatigue Cycling Effects

Longitudinal tensile test results from composite specimens that had been exposed to  $10^6$  fatigue cycles are shown in figure 12. Fatigue cycling increased the strength of the as-fabricated material (fig. 12(a)) by 30 percent and the elastic modulus by 12 percent; these properties attained the ROM values. Fatigue cycling of specimens which had been isothermally exposed for 2500 hours at 590 K (fig. 12(b)) returned the strength to the as-fabricated value, but the increase in stiffness was retained. Fatigue cycling (fig. 12(c)) after thermal cycling reduced the composite strength to 16 percent below the as-fabricated strength.

Breaking loads for individual fibers chemically removed from fatigue cycled specimens are shown in figure 13 and compared with fibers from unfatigued specimens. Fiber strength reduced in fabrication is restored by fatigue cycling as noted previously for the thermally exposed specimens. These results indicate that stress levels encountered during the fatigue cycling enhanced movement and annihilation of the quenched-in vacancies. The strength of fibers from thermally exposed and fatigue cycled specimens was approximately 10 percent less than the strength of fibers from specimens that were thermally exposed only. This is a small difference in a quantity with large variability but may indicate a detrimental cumulative effect of thermal exposure and fatigue cycling on fiber strength.

Fractographs of the fatigue cycled specimens are shown in figure 14. Comparison of as-fabricated specimen failure surfaces with fatigue (fig. 14(a)) and without fatigue (fig. 2) shows an apparent work hardening of the matrix material. There is less ductile necking of the matrix and flatter more brittle failure of the fibers. The overall failure surface is flatter and there is no apparent fatigue-induced damage. These same observations are true when comparing specimens exposed for 2500 hours at 590 K with fatigue (fig. 14(b)) and without fatigue (fig. 7(a)) and specimens thermally cycled with fatigue (fig. 14(c)) and without fatigue (fig. 11(a)). The effect of fatigue cycling on the specimens is more readily seen in the polished and etched longitudinal cross sections shown in figure 15. As-fabricated specimens with and without fatigue (fig. 15(a)) are identical in appearance and show no indication of fatigue-induced damage. Comparison of specimens exposed for 2500 hours

at 590 K with and without fatigue (fig. 15(b)) does show fatigue-induced damage. The specimen with fatigue has cracking in the matrix and fibers not present prior to fatigue cycling. The thermally cycled specimen without fatigue (fig. 15(c)) has extensive cracking in the matrix and fibers induced by the thermal expansion mismatch, but the addition of fatigue cycling causes increased damage and more fiber cracking.

These data indicate that the fatigue conditions imposed on the as-fabricated specimens had no detrimental effects on the composite but in fact restored the fiber properties and strengthened the composite. However, the combination of thermal exposure and fatigue cycling did adversely affect the composite properties by cracking both the matrix and the fibers. Although transverse tensile properties of the fatigue cycled specimens were not measured, they would certainly be further degraded by fatigue-induced matrix damage.

### SUMMARY OF RESULTS

Mechanical properties of as-fabricated  $\alpha\text{Al}_2\text{O}_3/\text{Al}$  composite material were measured, and the effects of elevated test temperature, continuous long duration thermal exposure, thermal cycling, and fatigue cycling were determined. Failure mechanisms and degradation mechanisms active in the material were investigated. The major findings were

1. The fabrication process severely degraded fiber strength, apparently caused by quenching in vacancies and accompanying stress fields introduced during the formation of a nonstoichiometric form of alumina. Each of the thermal exposure conditions and the fatigue cycle conditioning used in the study enhanced annihilation of the vacancies which relaxed the stress fields and restored the fiber strength.
2. Mechanical property tests conducted at temperatures up to 590 K did not show any significant temperature dependence of the fiber-dominated properties, but matrix-dominated properties were temperature dependent in the typical manner of aluminum. Comparing specific properties between 295 K and 590 K of the  $\alpha\text{Al}_2\text{O}_3/\text{Al}$  composite with the specific properties of several aerospace alloys and composite materials show that it is an attractive candidate for select applications.
3. Long duration isothermal exposure (up to 10 000 hours at 590 K) did not cause any measurable fiber-matrix interaction or fiber damage. It did, however, increase ductility in the matrix material and weaken the interface bond by the loss of lithium to a surface reaction forming lithium carbonate.
4. Thermal cycling caused matrix cracking as a result of the differential in thermal expansion between the fibers and matrix. Matrix cracks severely reduced transverse strength and induced stress concentrations in the fibers during longitudinal loading which caused premature fiber failure.

5. Fatigue cycling ( $10^6$  tension-tension cycles to two-thirds ultimate strength) of longitudinal tensile specimens did not cause any damage to the as-fabricated specimens but in fact increased their residual strength to the rule-of-mixtures value by restoring the fiber strength. Fatigue cycling of isothermally exposed specimens caused cracking in the matrix and fatigue cycling of thermally cycled specimens compounded matrix cracking. Matrix cracks induced stress concentrations in the fibers during mechanical loading and caused premature fiber failure.

Langley Research Center  
National Aeronautics and Space Administration  
Hampton, VA 23665  
December 2, 1980

## APPENDIX

### SYMBOLS

The following symbols appear in the tables and figures:

$\bar{E}_1$	mean longitudinal elastic modulus, GPa
$\bar{E}_2$	mean transverse elastic modulus, GPa
$\bar{G}_{12}$	mean shear modulus, GPa
$\bar{\nu}_{12}$	mean Poisson's ratio for transverse strain resulting from longitudinal stress
$\bar{\rho}$	mean density, $\text{kg}\cdot\text{m}^{-3}$
$\bar{\sigma}_{1t}$	mean ultimate longitudinal tensile strength, MPa
$\bar{\sigma}_{1c}$	mean ultimate longitudinal compression strength, MPa
$\bar{\sigma}_{tt}$	mean ultimate transverse tensile strength, MPa

## REFERENCES

1. Gitzen, Walter H., ed.: Alumina as a Ceramic Material. American Ceramic Soc., c.1970.
2. Tressler, Richard E.: Interfaces in Oxide Reinforced Metals. Interfaces in Metal Matrix Composites, Arthur G. Metcalfe, ed., Academic Press, Inc., 1974, pp. 285-328.
3. Mehan, R. L.; and Noone, M. J.: Nickel Alloys Reinforced With  $\alpha$ - $\text{Al}_2\text{O}_3$  Filaments. Metallic Matrix Composites, Kenneth G. Kreider, ed., Academic Press, Inc., 1974, pp. 159-227.
4. Lynch, C. T.; and Kershaw, J. P.: Metal Matrix Composites. Chemical Rubber Co., c.1972.
5. Champion, A. R.; Krueger, W. H.; Hartmann, H. S.; and Dhingra, A. K.: Fiber FP Reinforced Metal Matrix Composites. DuPont paper presented at Second International Conference on Composite Materials (Toronto, Canada), Apr. 16-20, 1978.
6. Prewo, K. M.: Fabrication and Evaluation of Low Cost Alumina Fiber Reinforced Metal Matrices. R77-912245-3 (Contract N00014-76-C-0035), United Technol. Res. Center, May 1977. (Available from DTIC as AD A040 953.)
7. Kim, W. H.; Koczak, M. J.; and Lawley, A.: Effects of Isothermal and Cyclic Exposures on Interface Structure and Mechanical Properties of FPC- $\text{Al}_2\text{O}_3$ /Aluminum Composites. Paper presented at Symposium on New Developments and Applications in Composites, 1978 TMS-AIME Fall Meeting (St. Louis, Missouri), Oct. 1978.
8. Yoshi-Yama, Tsuyoshi; Hasebe, Katsuhiko; and Mannami, Michi-Liko:  $\text{Al}_3\text{Li}$  Superlattice in Al-4.5wt.% Li Alloy. J. Phys. Soc. Japan, vol. 25, 1968, p. 908.
9. Ceresara, S.; Giarda, A.; and Sanchez, A.: Annealing of Vacancies and Ageing in Al-Li Alloys. Phil. Mag., vol. 35, no. 1, Jan. 1977, p. 97-110.
10. Ceresara, S.; Cocco, G.; Fagherazzi, G.; and Schiffini, L.: Determination of the  $\delta'$  Coherent Solvus in the Al-Li System by Small-Angle X-Ray Scattering. Phil. Mag., vol. 35, no. 2, Feb. 1977, pp. 373-378.
11. Mondolfo, L. F.: Aluminum Alloys: Structure and Properties. Butterworth Pub., Inc., 1976.
12. Greszczuk, L. B.: Shear-Modulus Determination of Isotropic and Composite Materials. Composite Materials: Testing and Design, Spec. Tech. Publ. No. 460, American Soc. Testing Mater., c.1969., pp. 140-149.
13. Clark, Ronald K.; and Lisagor, W. Barry: Effects of Method of Loading and Specimen Configuration on Compressive Strength of Graphite/Epoxy Composite Materials. NASA TM-81796, 1980.

14. Advanced Composites Design Guide. Volume IV - Materials. Third ed., Air Force Materials Lab., U.S. Air Force, Jan. 1973. (Available from DTIC as AD-916 682L.)
15. Herring, Harvey W.: Fundamental Mechanisms of Tensile Fracture in Aluminum Sheet Unidirectionally Reinforced With Boron Filament. NASA TR R-383, 1972.
16. Teichner, S.; Juillet, F.; and Arghiropoulos, B.: Sur une Nouvelle Forme d'Alumine Colorée et Non Stoechiometrique. Bull. Soc. Chim., 1959, pp. 1491-1495.
17. Juillet, Francois; Prettre, Marcel; and Teichner, Stanislas: Evolution Texturale de L'alumine Coloree Non Stoechiometrique. Compt. Rend. Acad. Sci., t. 249, no. 15, Oct. 12, 1959, pp. 1356-1358.
18. Arghiropoulos, Basile; Elston, Jean; Juillet, Francois; and Teichner, Stanislas: Sur une Nouvelle Methode de Preparation de L'alumine Coloree Non Stoechiometrique. Compt. Rend. Acad. Sci., t. 249, no. 23, Dec. 9, 1959, pp. 2549-2551.
19. Arghiropoulos, Basile; Juillet, Francois; Prettre, Marcel; and Teichner, Stanislas: Evolution Structurale et Proprietes Electriques de L'alumine Coloree Non Stoechiometrique. Compt. Rend. Acad. Sci., t. 249, no. 19, Nov. 9, 1959, pp. 1895-1897.
20. Mechanical Properties Data Center, Battelle Columbus Lab.: Aerospace Structural Metals Handbook - 1980 Publication. (Formerly AFML-TR-68-115.)
21. Olsen, George C.: Thermal Exposure Effects on the Mechanical Properties of a Polycrystalline Alumina Fiber/Aluminum Matrix Composite. The Enigma of the Eighties: Environment, Economics, Energy, Volume 24 of National SAMPE Symposium and Exhibition, Soc. Advance. Mater. & Process Eng., c.1979, pp. 1069-1080.



TABLE I.- CONFIGURATIONS OF UNIDIRECTIONAL  $\text{Al}_2\text{O}_3/\text{Al}$  COMPOSITE

TEST SPECIMENS

Test	Fiber orientation	Specimen dimensions, mm			
		Length	Width	Thickness	Gage length
Tension	0°	150	12.7	2.6	50.8
	45°	150	12.7	2.6	50.8
	90°	100	25.4	2.6	25.4
Compression	0°	150	6.4	2.6	12.7

TABLE II.- MECHANICAL PROPERTY TESTS

Test	Fiber orientation	Standard or reference	Properties reported	Cross-head speed, mm/sec
Tension	0°	ASTM D-3552	$\bar{E}_1, \bar{\sigma}_{1t}, \bar{\nu}_{12}$	0.0085
	45°	ASTM D-3552 and Ref. 12	$\bar{G}_{12}$	.0085
	90°	ASTM D-3552	$\bar{E}_2, \bar{\sigma}_{tt}$	.0085
Compression	0°	<sup>a</sup> ASTM D-3410	$\bar{\sigma}_{1c}$	0.0004

<sup>a</sup>Standard for resin matrix composites.

TABLE III.-  $\alpha\text{Al}_2\text{O}_3/\text{Al}$  COMPOSITE LONGITUDINAL AND TRANSVERSE TENSILE TEST RESULTS

Specimen history	Test temperature, K	Longitudinal		Transverse	
		Ultimate stress, MPa	Elastic modulus, GPa	Ultimate stress, MPa	Elastic modulus, GPa
As fabricated	295	537	213	188	171
		543	207	187	150
		575	209	184	159
	500	541	219	118	123
		455	224	118	119
		654	(a)	110	108
	590	548	221	74	110
		510	229	72	130
		493	220	73	106
2500 hr at 590 K	295	637	230	119	130
		658	228	114	130
		601	226	106	141
5000 hr at 590 K	295	547	216	80	108
		510	229	77	104
		505	210	80	(a)
10 000 hr at 590 K	295	528	227	70	(a)
		513	226	70	106
		515	223		
6000 cycles between 200 K and 590 K	295	557	219	69	(b)
		630	226	60	
		637	219	70	
$10^6$ fatigue cycles	295	704	234		
		744	233		
		697	236		
2500 hr at 590 K and $10^6$ fatigue cycles	295	509	(a)		
		563	234		
		508	(a)		
6000 cycles between 200 K and 590 K and $10^6$ fatigue cycles	295	454	206		
		469	202		

<sup>a</sup>Strain gages failed.

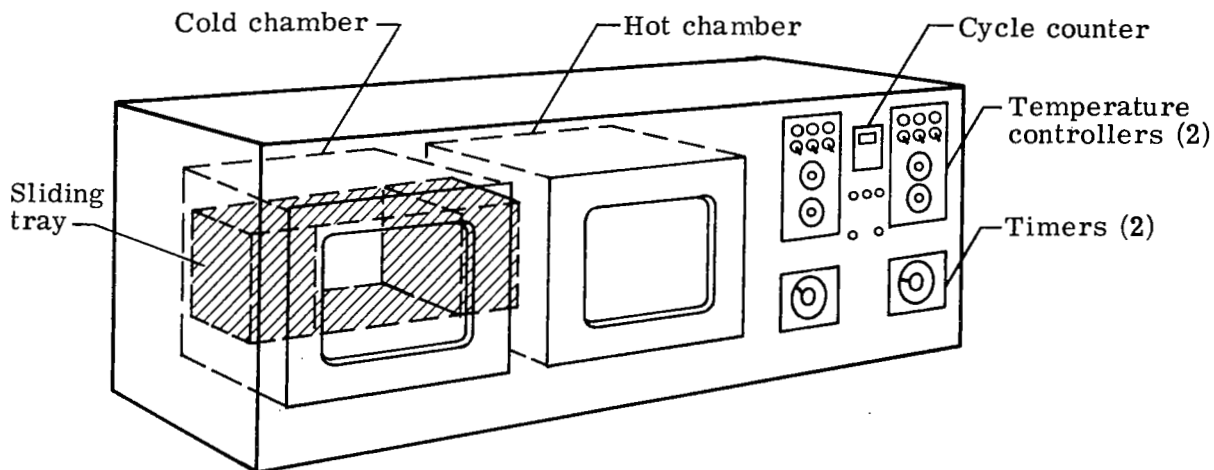
<sup>b</sup>Insufficient elastic zone.

TABLE IV.-  $\alpha\text{Al}_2\text{O}_3/\text{Al}$  COMPOSITE COMPRESSION AND SHEAR  
MODULUS TEST RESULTS

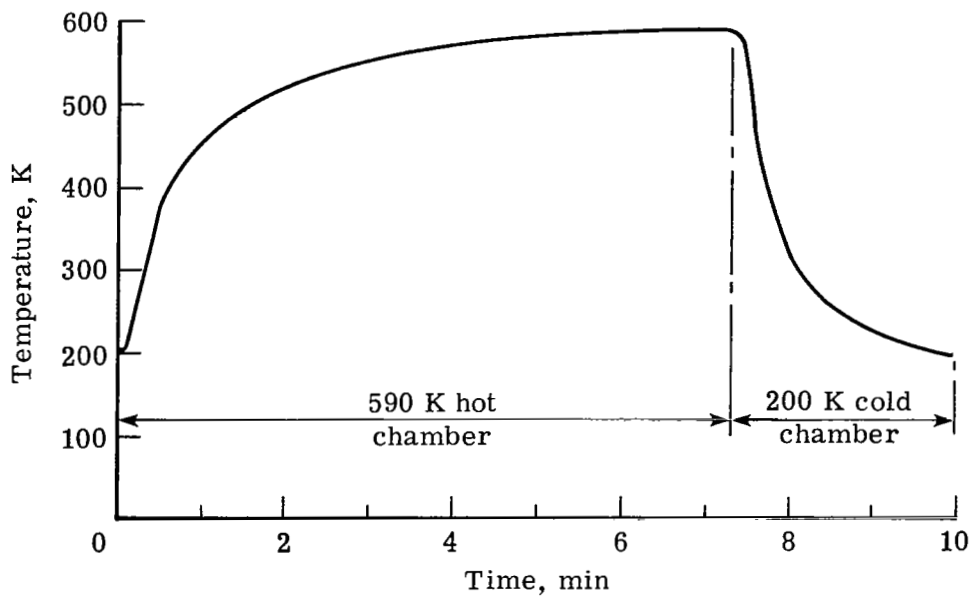
Specimen history	Test temperature, K	Compression		Shear modulus, GPa
		Ultimate stress, MPa	Elastic modulus, GPa	
As fabricated	295	2781	216	58.6
		2465	209	56.5
		2636	215	58.3
	500	1932	202	64.0
		1470	194	54.7
		1159	190	54.2
	590	1625	207	50.8
		962	202	45.4 51.4
	2500 hr at 590 K	295	2152	228
2276			226	61.0
2122			231	61.2
6000 cycles between 200 K and 590 K	295	1831	219	30.6
		1812	219	28.0
		1767	235	31.1

TABLE V.- MECHANICAL PROPERTIES OF AS-FABRICATED  $\alpha\text{Al}_2\text{O}_3/\text{Al}$  COMPOSITE

Longitudinal tensile strength, $\bar{\sigma}_{1t}$ , MPa . . . . .	522
Longitudinal elastic modulus, $\bar{E}_1$ , GPa . . . . .	210
Transverse tensile strength, $\bar{\sigma}_{tt}$ , MPa . . . . .	186
Transverse elastic modulus, $\bar{E}_2$ , GPa . . . . .	160
Longitudinal compressive strength, $\bar{\sigma}_{1c}$ , MPa . . . . .	2627
Shear modulus, $\bar{G}_{12}$ , GPa . . . . .	58
Poisson's ratio, $\bar{\nu}_{12}$ . . . . .	0.27
Density, $\bar{\rho}$ , $\text{kg}\cdot\text{m}^{-3}$ . . . . .	3203

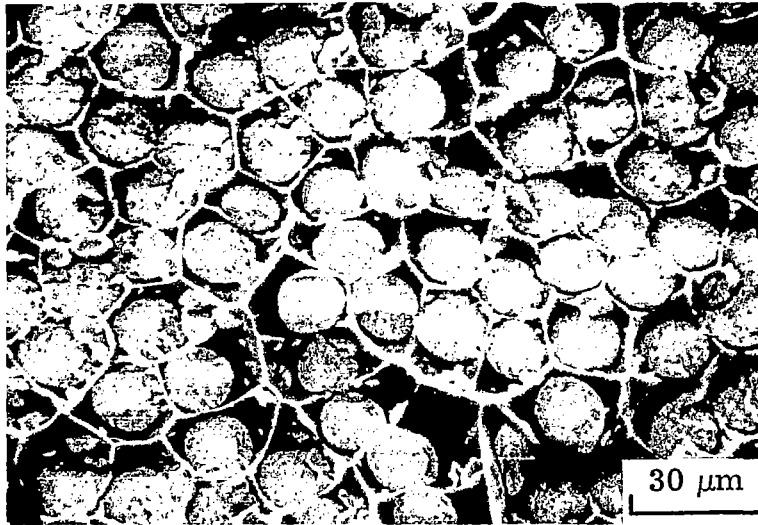


(a) Thermal cycling apparatus.

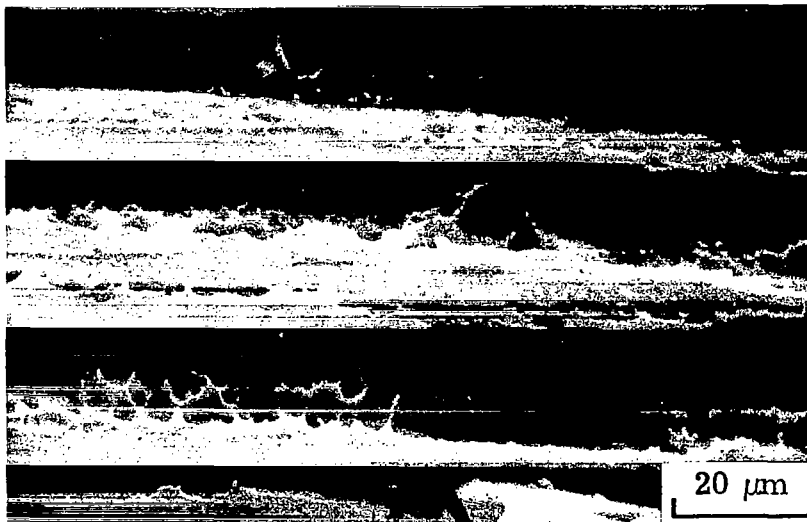


(b) Typical specimen temperature history for one cycle.

Figure 1.- Cyclic thermal exposure.



(a) Longitudinal.



(b) Transverse.

Figure 2.- Typical fracture surfaces of as-fabricated  $\alpha\text{Al}_2\text{O}_3/\text{Al}$  composite specimens. L-80-220

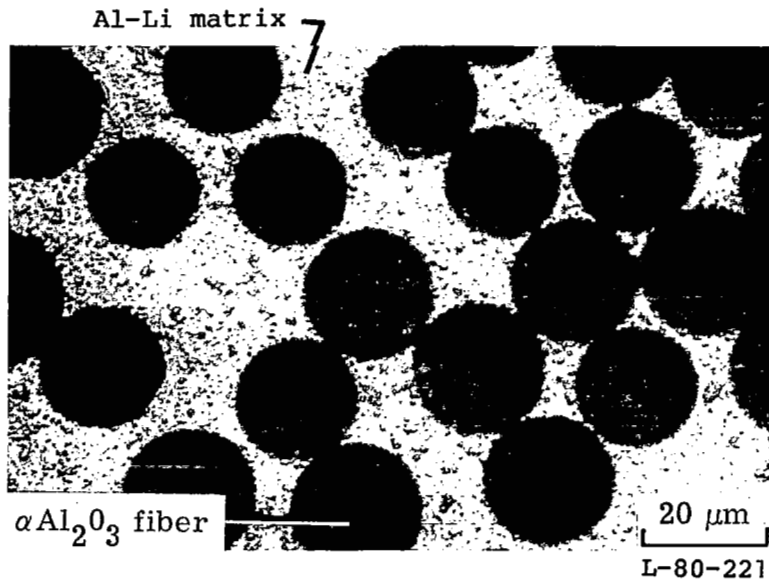


Figure 3.-Typical cross section of as-fabricated  $\alpha\text{Al}_2\text{O}_3/\text{Al}$  composite specimens.

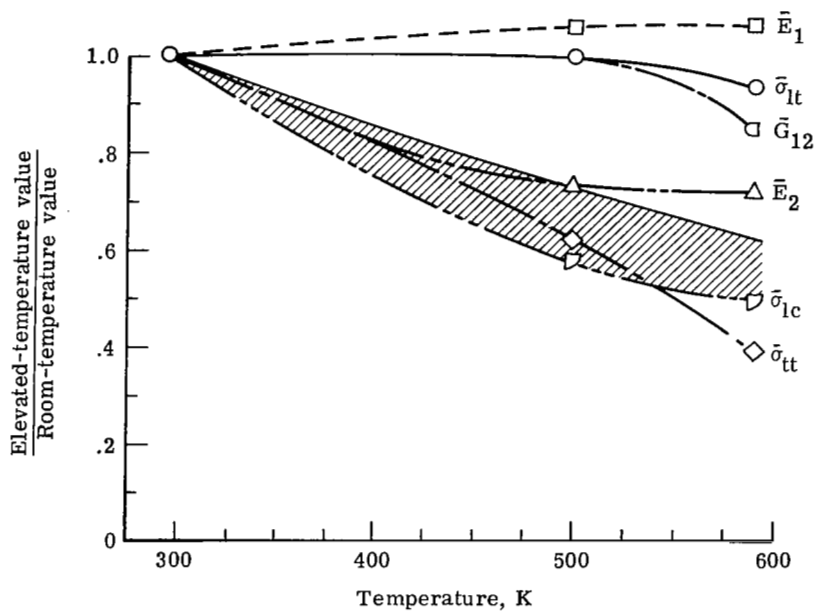
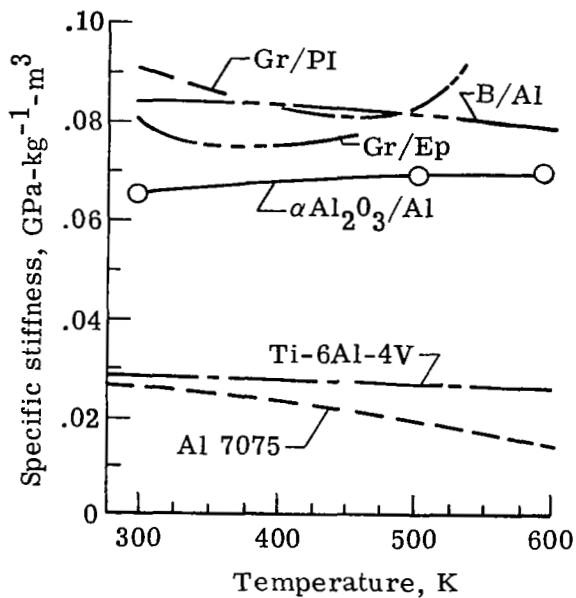
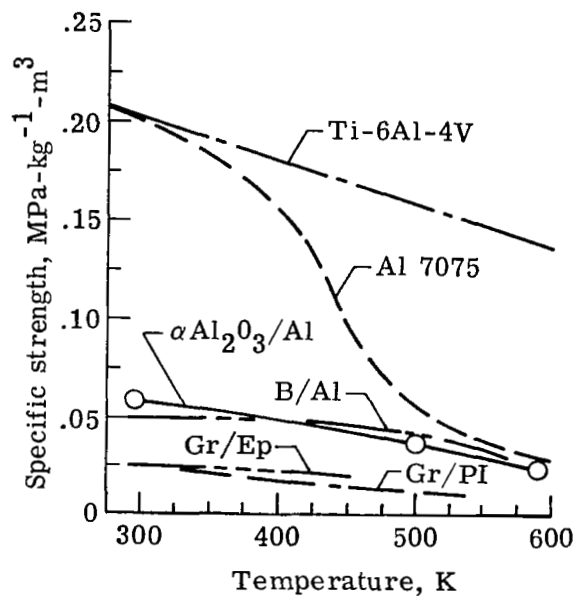


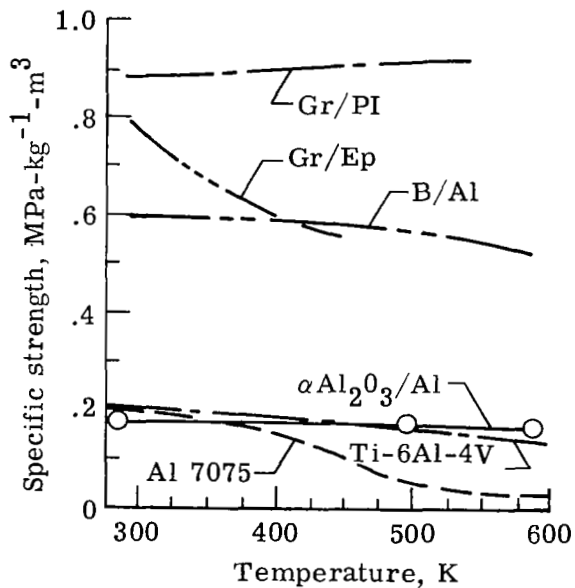
Figure 4.- Effect of elevated test temperature on as-fabricated  $\alpha\text{Al}_2\text{O}_3/\text{Al}$  composite material, normalized by room-temperature properties.



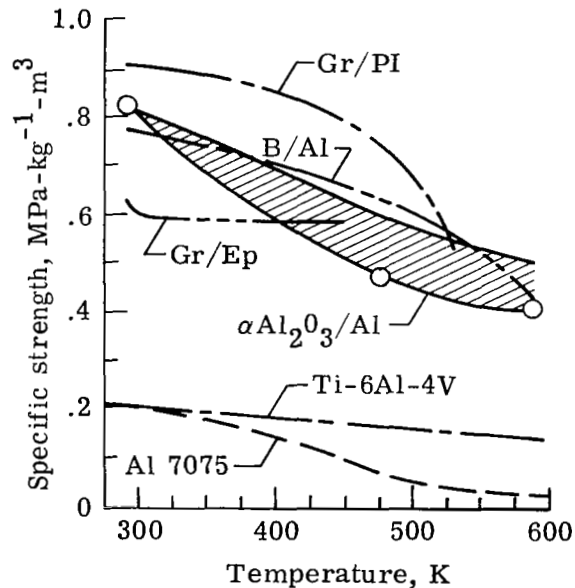
(a) Specific stiffness.



(b) Specific transverse tensile strength.



(c) Specific longitudinal tensile strength.



(d) Specific longitudinal compression strength.

Figure 5.- Specific properties versus test temperature of  $\alpha\text{Al}_2\text{O}_3/\text{Al}$  composite compared with Al 7075, Ti-6Al-4V, B/Al, Gr/Ep, and Gr/PI.

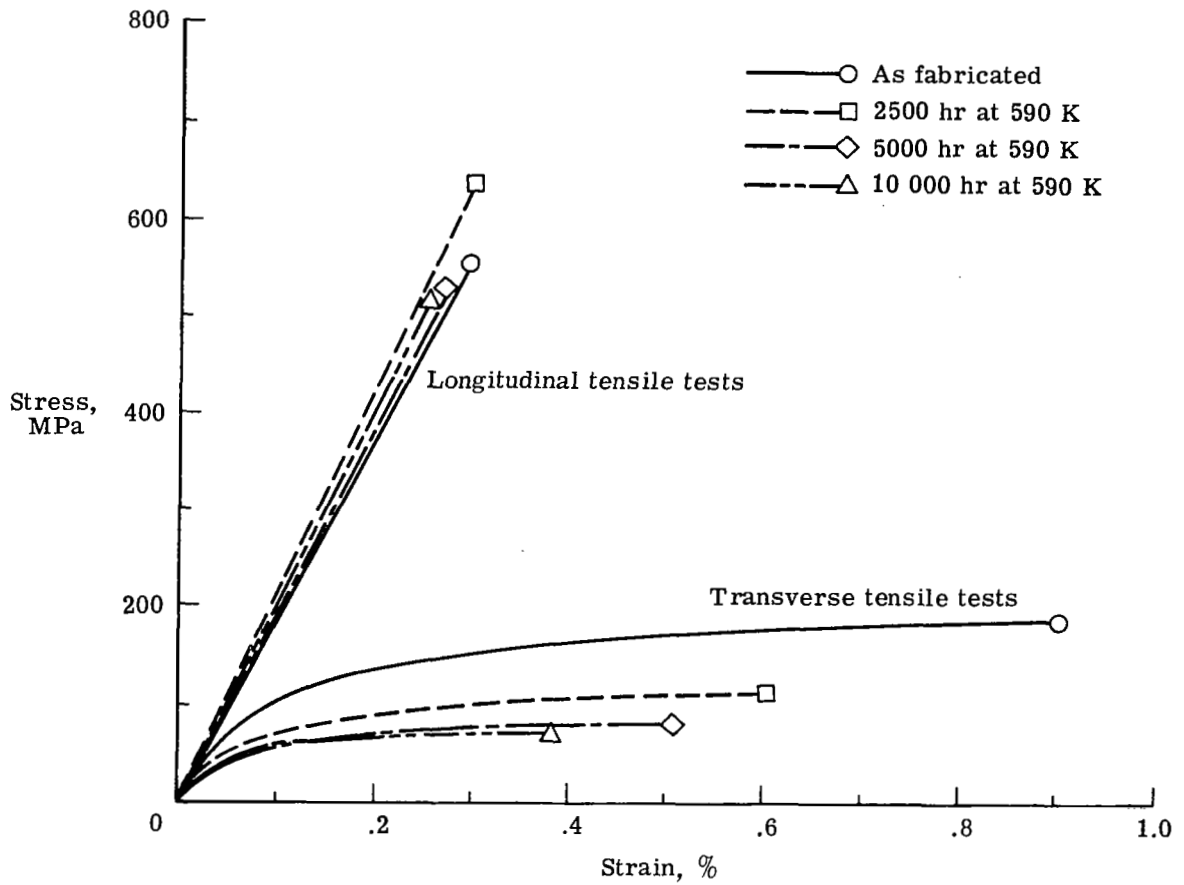
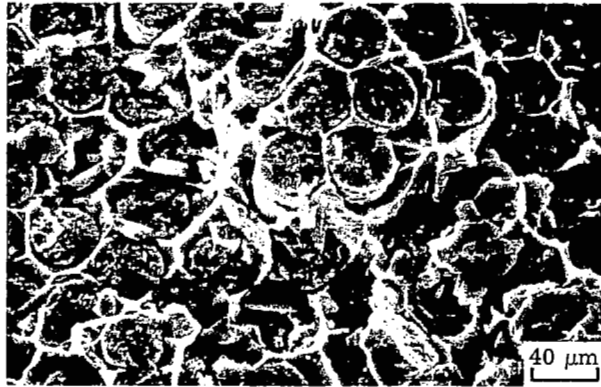
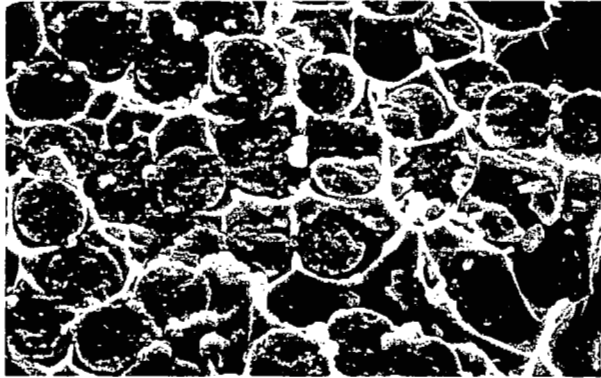


Figure 6.- Typical room-temperature longitudinal and transverse stress-strain curves for  $\alpha\text{Al}_2\text{O}_3/\text{Al}$  composite material exposed at 590 K.

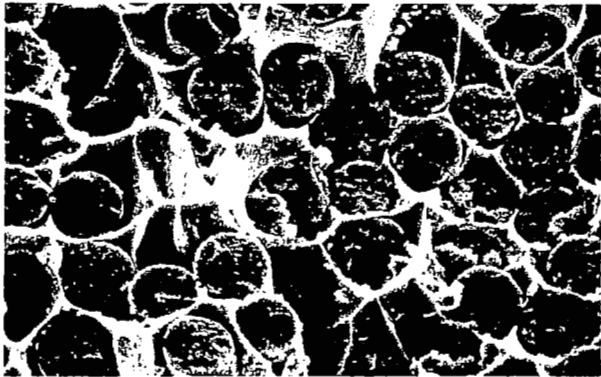




(a) 2500 hours.

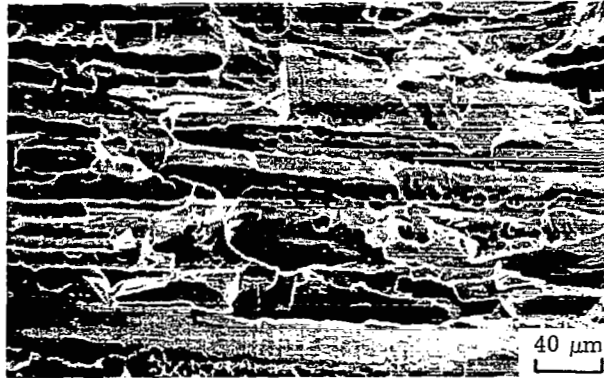


(b) 5000 hours.

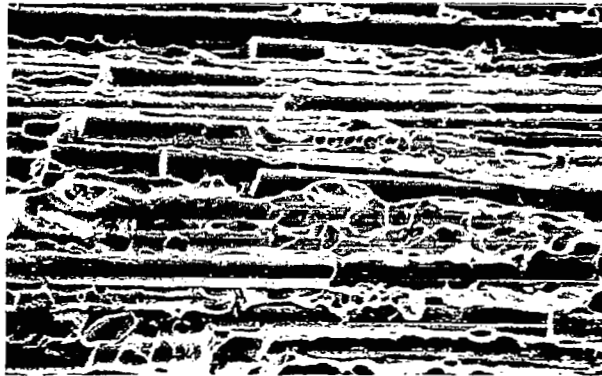


(c) 10 000 hours.

Figure 7.- Typical longitudinal tensile fracture surfaces of  $\alpha\text{Al}_2\text{O}_3/\text{Al}$  composite specimens thermally exposed at 590 K. L-80-222



(a) 2500 hours.



(b) 5000 hours.



(c) 10 000 hours.

L-80-223

Figure 8.- Typical transverse tensile fracture surfaces of  $\alpha\text{Al}_2\text{O}_3/\text{Al}$  composite specimens thermally exposed at 590 K.

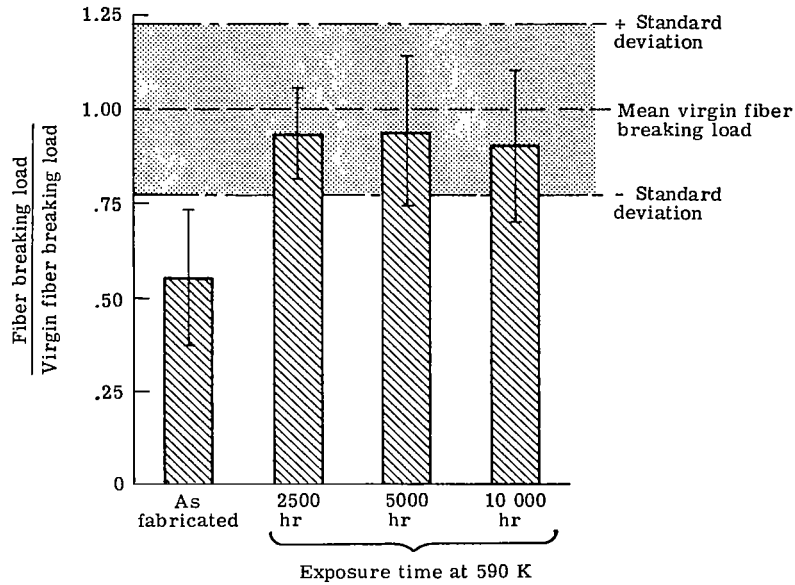


Figure 9.-  $\alpha\text{Al}_2\text{O}_3$  fiber breaking loads after removal from composite specimens thermally exposed at 590 K.

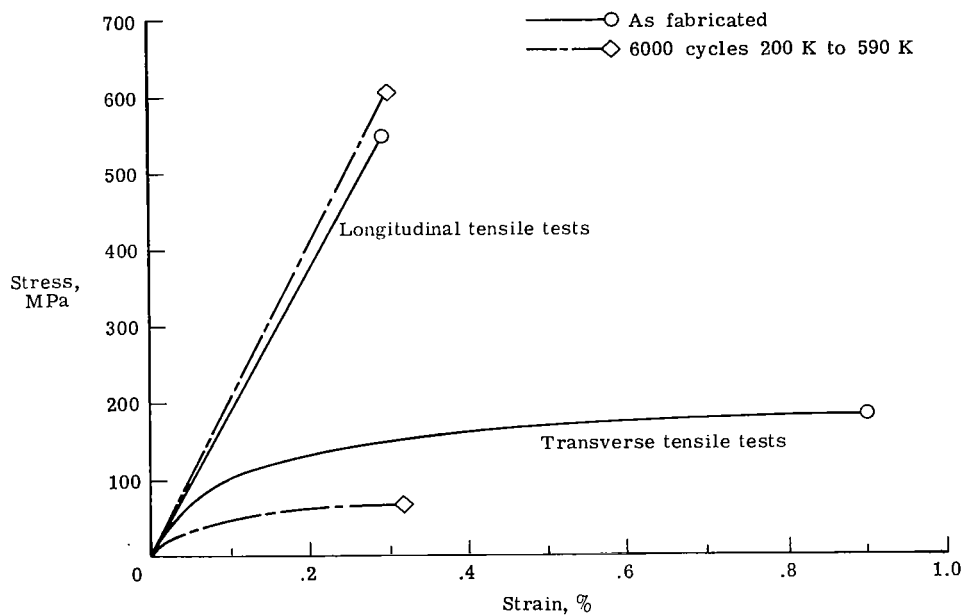


Figure 10.- Typical room-temperature longitudinal and transverse stress-strain curves for  $\alpha\text{Al}_2\text{O}_3/\text{Al}$  composite material after 6000 thermal cycles between 200 K and 590 K.



(a) Longitudinal.



(b) Transverse.

Figure 11.- Typical fracture surfaces of  $\alpha\text{Al}_2\text{O}_3/\text{Al}$  composite specimens after 6000 thermal cycles between 200 K and 590 K. L-80-224

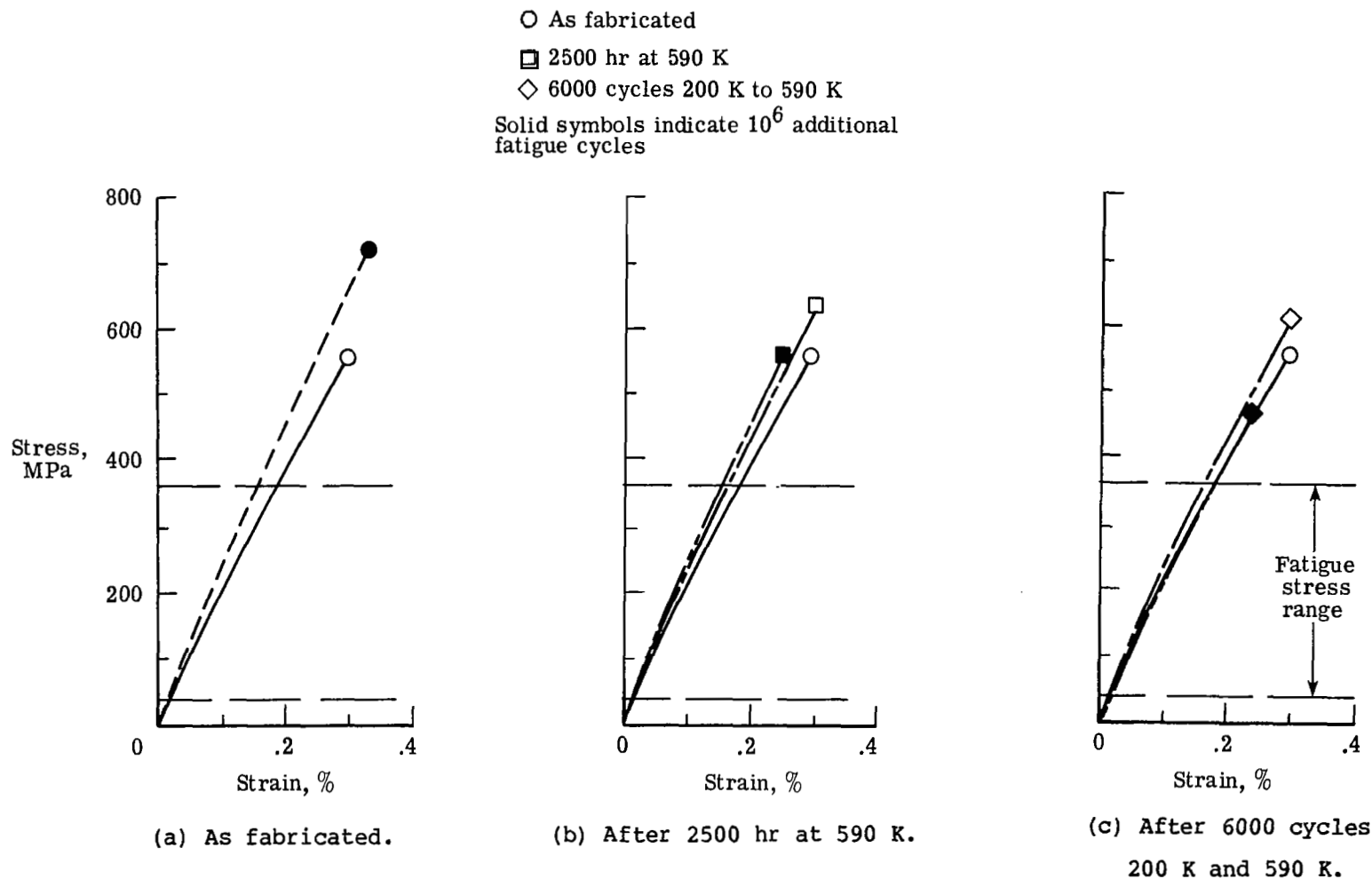


Figure 12.- Typical room-temperature longitudinal stress-strain curves for  $\alpha\text{Al}_2\text{O}_3/\text{Al}$  composite material after  $10^6$  fatigue cycles.

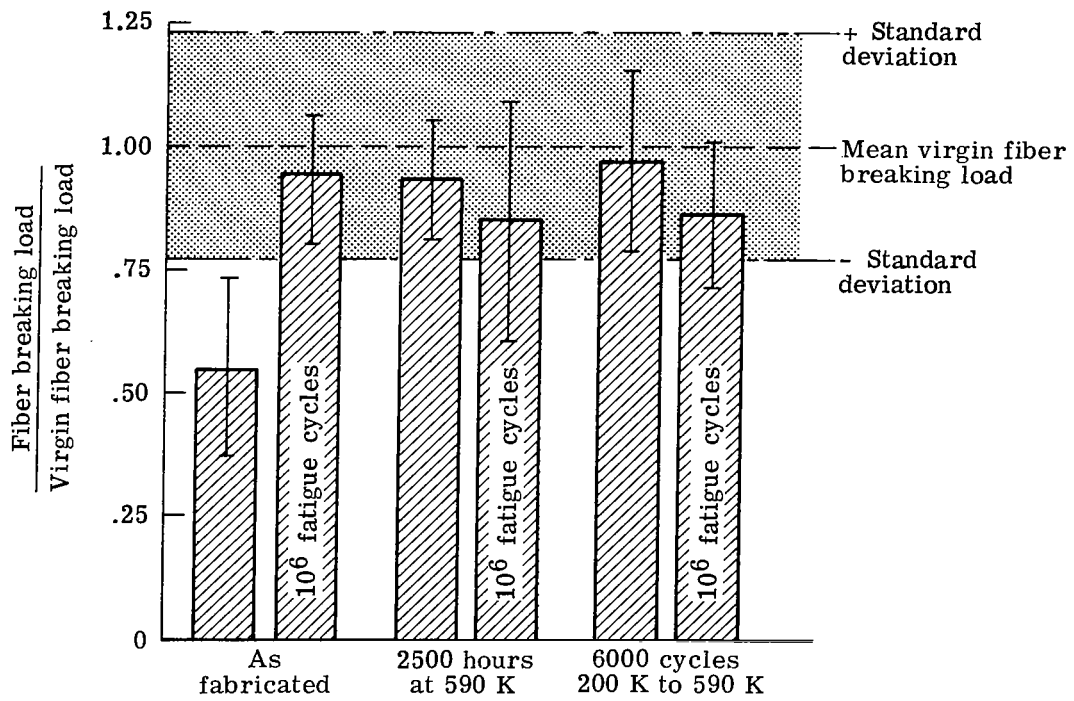
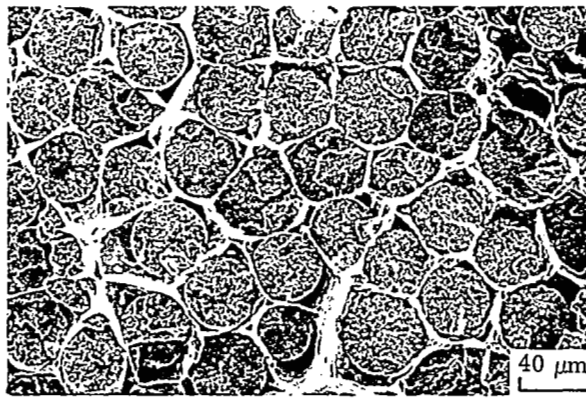
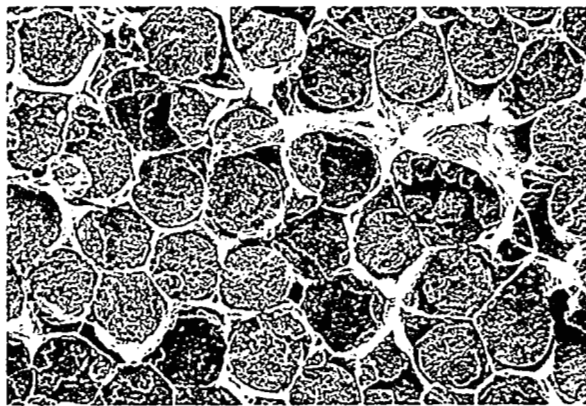


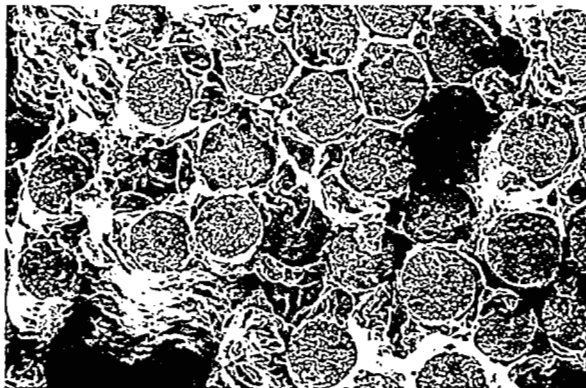
Figure 13.-  $\alpha\text{Al}_2\text{O}_3$  fiber breaking loads after removal from composite specimens exposed to  $10^6$  fatigue cycles.



(a) As fabricated.



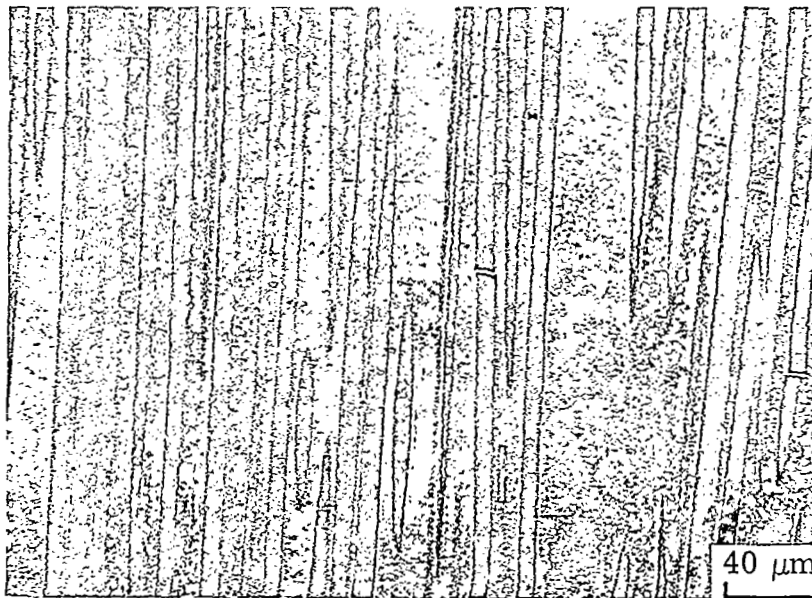
(b) 2500 hours at 590 K.



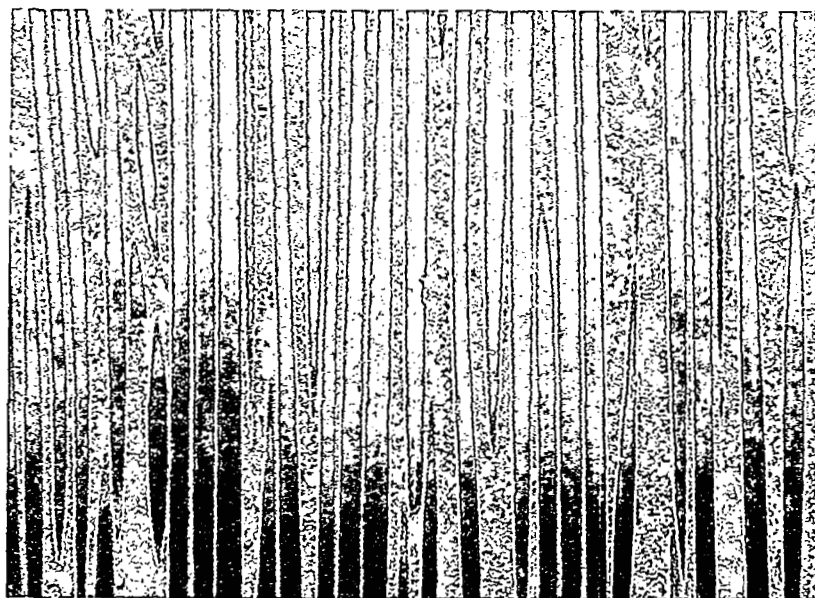
(c) 6000 thermal cycles between  
200 K and 590 K.

Figure 14.- Typical longitudinal tensile fracture surfaces of  $\alpha\text{Al}_2\text{O}_3/\text{Al}$  composite specimens after  $10^6$  fatigue cycles.

L-80-225



Without fatigue



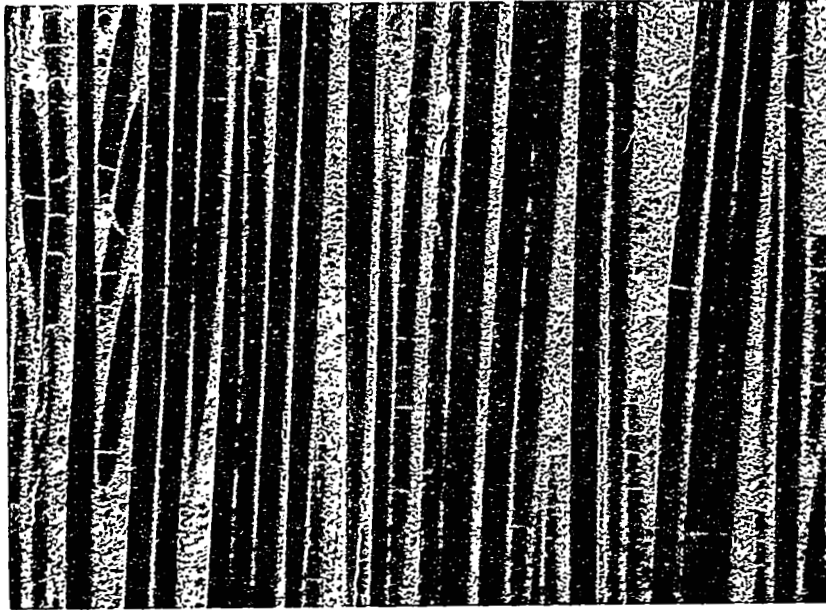
With fatigue

L-80-226

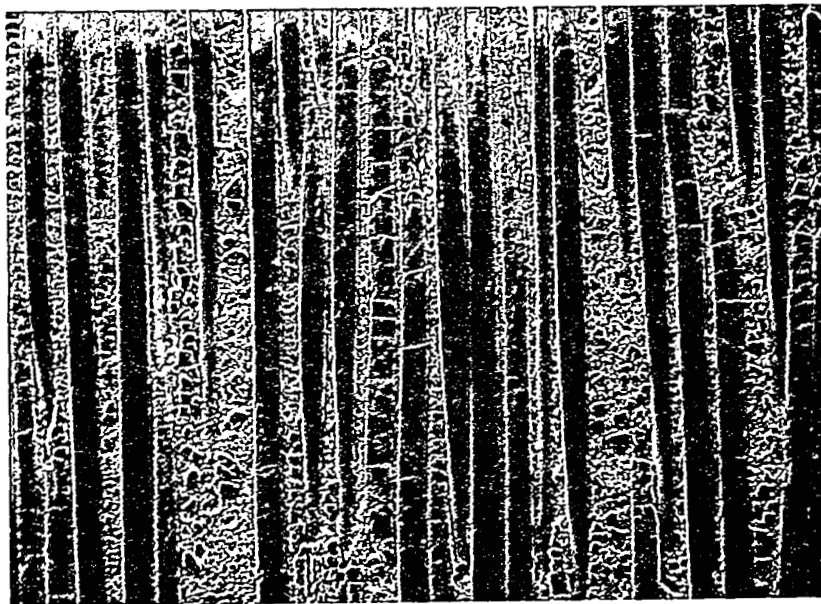
(a) As fabricated.

Figure 15.- Typical transverse cross sections of polished and etched  $\alpha\text{Al}_2\text{O}_3/\text{Al}$  composite specimens before and after exposure to  $10^6$  fatigue cycles.





Without fatigue

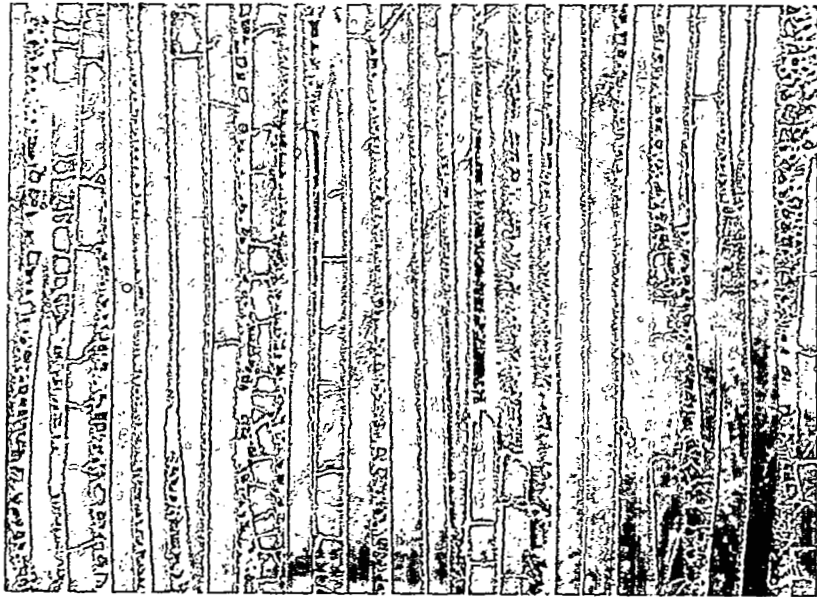


With fatigue

L-80-227

(b) 2500 hours at 590 K.

Figure 15.- Continued.



Without fatigue



With fatigue

L-80-228  
(c) 6000 thermal cycles between 200 K and 590 K.

Figure 15.- Concluded.

1. Report No. NASA TP-1795		2. Government Accession No.		3. Recipient's Catalog No.	
4. Title and Subtitle EFFECTS OF TEMPERATURE, THERMAL EXPOSURE, AND FATIGUE ON AN ALUMINA/ALUMINUM COMPOSITE				5. Report Date December 1980	
				6. Performing Organization Code 506-53-23-01	
7. Author(s) George C. Olsen				8. Performing Organization Report No. L-14074	
9. Performing Organization Name and Address NASA Langley Research Center Hampton, VA 23665				10. Work Unit No.	
				11. Contract or Grant No.	
12. Sponsoring Agency Name and Address National Aeronautics and Space Administration Washington, DC 20546				13. Type of Report and Period Covered Technical Paper	
				14. Sponsoring Agency Code	
15. Supplementary Notes					
16. Abstract <p>The mechanical properties and microstructure of an aluminum matrix/polycrystalline alumina fiber composite material were experimentally studied. The effects of fabrication, isothermal exposure (up to 10 000 hours at 590 K), thermal cycling (6000 cycles between 200 K and 590 K), fatigue (<math>10^6</math> tension-tension cycles) were determined by mechanical testing and metallurgical analysis. The fabrication process severely degraded the fiber strength by reducing the alumina to a nonstoichiometric form and quenching in the resultant vacancies and stress fields. However, isothermal exposure, thermal cycling, and fatigue cycling all restored the fiber strength by enhancing vacancy annihilation. Comparison of the as-fabricated material with other aerospace materials show that it is an attractive candidate for select applications. Long duration isothermal exposure weakened the matrix by overaging and through the diffusional loss of lithium to a surface reaction forming lithium carbonate. Thermal cycling initiated cracks in the matrix and fibers. Tension-tension fatigue cycling caused no apparent damage to the as-fabricated material but in fact, strengthened it to the rule-of-mixtures value. Fatigue cycling after thermal exposure did have a cumulative damage effect.</p>					
17. Key Words (Suggested by Author(s)) Metal matrix composite Alumina-aluminum Thermal degradation Thermal fatigue Mechanical fatigue			18. Distribution Statement Unclassified - Unlimited  Subject Category 24		
19. Security Classif. (of this report) Unclassified	20. Security Classif. (of this page) Unclassified	21. No. of Pages 32	22. Price A03		

National Aeronautics and  
Space Administration

Washington, D.C.  
20546

Official Business

Penalty for Private Use, \$300

THIRD-CLASS BULK RATE

Postage and Fees Paid  
National Aeronautics and  
Space Administration  
NASA-451



17 1 1U,C, 121980 S00903DS  
DEPT OF THE AIR FORCE  
AF WEAPONS LABORATORY  
ATTN: TECHNICAL LIBRARY (SUL)  
KIRTLAND AFB NM 87117

**NASA**

POSTMASTER: If Undeliverable (Section 158  
Postal Manual) Do Not Return

---